# Polarization-dependent photoemission electron microscopy for domain imaging of inorganic and molecular materials 0

Cite as: J. Chem. Phys. 161, 110901 (2024); doi: 10.1063/5.0225765 Submitted: 26 June 2024 • Accepted: 11 August 2024 • Published Online: 16 September 2024











Atreyie Ghosh, Doseph L. Spellberg, and Sarah B. King, and Sarah B. Ki



## **AFFILIATIONS**

- <sup>1</sup> James Franck Institute, The University of Chicago, Chicago, Illinois 60637, USA
- <sup>2</sup>Department of Chemistry, The University of Chicago, Chicago, Illinois 60637, USA
- a) Author to whom correspondence should be addressed: sbking@uchicago.edu

#### **ABSTRACT**

Polarization-dependent photoemission electron microscopy (PD-PEEM) exploits spatial variation in the optical selection rules of materials to image domain formation and material organization on the nanoscale. In this Perspective, we discuss the mechanism of PD-PEEM that results in the observed image contrast in experiments and provide examples of a wide range of material domain structures that PD-PEEM has been able to elucidate, including molecular and polymer domains, local electronic structure and defect symmetry, (anti)ferroelectricity, and ferromagnetism. In the end, we discuss challenges and new directions that are possible with this tool for probing domain structure in materials, including investigating the formation of transient ordered states, multiferroics, and the influence of molecular and polymer order and disorder on excited state dynamics and charge transport.

Published under an exclusive license by AIP Publishing. https://doi.org/10.1063/5.0225765

## I. INTRODUCTION

Domain formation in solid-state materials is extremely common. Domains can be formed due to variations in molecular alignment, 1,2 crystallization, 3 bond distortions, 4 and spin alignment.<sup>5</sup> Bond distortion and spin ordering can result in properties such as (anti)ferroelectricity and (anti)ferromagnetism, while variations in molecular alignment and crystallinity can modify the efficiency of processes such as photoinduced current and electrocatalysis. 1,6 Depending on the energy for domain alignment/misalignment and opportunities for external control, domains can be used for energy<sup>7</sup> and information storage, <sup>8-10</sup> sensors, <sup>11</sup> and electronics.12,

Some of the most common domain-forming materials are molecular crystals, 14 polymers, 2,15 ferroelectrics, 4 ferromagnets, 16 and multiferroics.  $^{17}$  The size of these domains can range from a few nanometers to micrometers. However, a critical issue in investigating and controlling materials that form domains is that, for many materials, the domains are quite difficult to observe. Developing techniques that can simultaneously image domains and characterize their properties and dynamics across a wide range of samples has been extremely challenging. To begin with, techniques such as

grazing-incidence small-angle x-ray scattering (GISAXS)<sup>18</sup> and lowenergy electron diffraction (LEED)<sup>19</sup> can quantify whether domains have formed in a material and the average symmetries of different domains with respect to each other. However, these techniques average over a fairly large interaction volume and contain only moderate local structure information.

Scanning probe microscopies, such as magnetoresponse force microscopy (MFM),<sup>20</sup> piezoresponse force microscopy (PFM),<sup>21</sup> and near-field scanning optical microscopy (NSOM),<sup>22</sup> are widely used methods to identify domains in materials. These techniques use a modified atomic force microscopy (AFM) tip that raster-scans across a material, collecting information through the tip-sample interactions as a function of space, which provides details of variation in the structural, electronic, or magnetic properties of a material on the nanoscale. NSOM can also probe light interactions with the AFM tip, but light polarization control is extremely challenging and is an active area of research.<sup>23,24</sup> The biggest benefits of these techniques include their excellent spatial resolution on the order of <10 nm,25 operation under ambient conditions, and the wideflexibility of sample conditions and substrates that can be used for investigation. PFM and MFM are successful at imaging out of plane ferroelectricity and ferromagnetism, respectively. These techniques, however, have limitations in characterizing in-plane effects, such as antiferroelectricity<sup>26</sup> and antiferromagnetism,<sup>27</sup> due to vanishing resulting polarization and magnetization, respectively. Furthermore, since these three techniques all involve raster scanning with a tip, the constraints of limited area scanning and long scan times exist.

Electron microscopies, such as (scanning) transmission electron microscopy (STEM) and 4D-STEM, can provide detailed structural information about a material with atomic resolution but have downsides when considering the electronic structure and symmetry. It can also be challenging to accurately interpret magnetic effects in these techniques due to the contribution of electron scattering effects from local structural changes.<sup>28,29</sup> In addition, molecular and polymer systems can be easily damaged by the high energy electron beam involved in these methods.<sup>30</sup> Low-energy electron microscopy (LEEM) can probe the spatial variation of the near-Fermi level electronic structure and, combined with micro-LEED, enables structural characterization of different domains.<sup>31,32</sup> However, LEEM is a structurally sensitive method rather than a chemically sensitive method, and therefore, it is often combined with photoemission electron microscopy (PEEM), as shown in Fig. 1(a).<sup>33</sup>

Optical microscopy approaches to investigating domain formation rely on differences in light absorption, emission, or scattering as a function of real space. Techniques such as optical birefringence, second-harmonic-generation/sum-frequency-generation microscopy, and Raman and photoluminescence (PL) microscopy have been used to probe domain formation. <sup>22,35–37</sup> These techniques can be operated under ambient conditions or even at elevated pressures and do not require ultra-high vacuum sample conditions. Furthermore, there are often few substrate requirements for these

kinds of techniques—conductive or electron transmissive substrates are typically not required—making optical techniques extremely versatile. Optical microscopy can also be used to probe the dynamics of domains in materials, for example, by using light with an ultrashort pulse duration for stroboscopic imaging. However, in most cases, optical microscopy methods are limited by the optical diffraction limit of several hundreds of nanometers—larger than typical domains in many materials. In addition, optical microscopy measures optical transitions rather than measuring electronic structure directly with respect to a universal energy, such as the Fermi level.

This Perspective puts forward polarization-dependent photoe-mission electron microscopy (PD-PEEM) as a technique for imaging domain formation in a broad range of materials. PD-PEEM is extremely well suited for probing domain structure, electronic structure, and excited state dynamics due to its combination of photon interrogation with electron imaging, which allows us to leverage properties of light such as photon energy, polarization, and controllable pulse duration to image domains and dynamics in materials on the nanoscale.

#### II. BACKGROUND

## A. Photoemission electron microscopy

Photoemission electron microscopy (PEEM) is an electron microscopy technique that resolves spatial variation in photoemission intensity and energy to image materials on the nanoscale. <sup>40</sup> PEEM takes advantage of the photoelectric effect to create an electron image of a material's surface. The absorption of a photon with sufficient energy results in the emission of an electron from

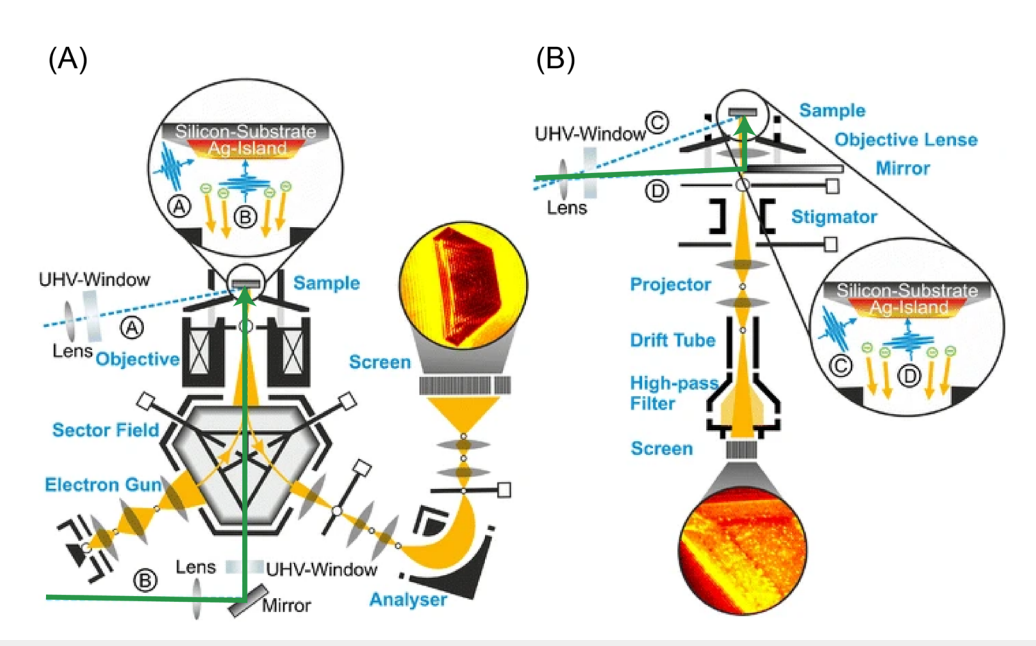


FIG. 1. Two main instrumental designs that enable the normal incidence laser excitation that is required for PD-PEEM. Design (a) illuminates through the magnetic mirror used in LEEM/PEEM instruments that enables imaging via both scattered and photoemitted electrons. Design (b) uses a small rhodium mirror that is placed in the electron column to enable normal incidence. Both normal incidence beam-paths are highlighted in green. Reproduced with permission from Kahl *et al.*, Plasmonics **9**, 1401 (2014).<sup>34</sup> Copyright 2014 Springer Nature Publishing.

a material surface with a defined kinetic energy  $E_{KE}$ . The kinetic energy is defined as  $E_{KE} = hv - E_B = hv - \Phi + (E - E_F)$ , where hv is the incident photon energy and  $E_B$  is the electron's binding energy, which can be decomposed into the work function,  $\Phi$ , the initial state energy, E, and the Fermi level,  $E_F$ . There are several different ways that image contrast can be achieved in PEEM based on this mechanism of image formation. Spatial variations in the work function or electronic structure of a material on the nanoscale will necessarily result in variations in the kinetic energy and intensity of electrons emitted from a sample, providing image contrast. However, in the case of a continuous material with the same work function and same electronic structure—such as in the case of material domains that have the identical electronic structure—this aspect of PEEM will provide no image contrast. Instead, one relies on the photon interaction with the material and the role of polarization in order to provide image contrast in PD-PEEM.

Similar to other electron microscopy techniques, such as transmission electron microscopy (TEM) and scanning electron microscopy (SEM), PEEM is fundamentally bounded by the electron diffraction limit, which is sub-nm. After correcting for aberrations in the electron microscope, a spatial resolution of <10 nm can be achieved in the instrument in PEEM mode. 41,42 While SEM and TEM impinge electrons on a sample and then detect emitted, scattered, or transmitted electrons, PEEM impinges photons on a sample and then detects the emitted electrons in wide-field imaging. It combines the tunability of light/photon interrogation with the spatial resolution of electron detection in a wide-field image. It is precisely this photon-interrogation that enables PD-PEEM to image domains in a wide range of contexts.

In addition to the energy requirements for the emission of an electron, there must be a sufficiently strong optical transition from the occupied electronic states to the electronic states above the vacuum that leads to the emission of an electron. These transitions can be achieved with either a single photon [1-photon photoemission (1PPE)] or with multiple photons [n-photon photoemission (nPPE)]. Each photon interaction allows for variation in the optical selection rules to provide contrast in PEEM. Three different pictures of PEEM selection rules are described in Sec. II B, where each of those cases is useful for predicting how PD-PEEM can be applied to a different type of domain imaging. In particular, in PD-PEEM, we exploit a variation in the selection rules with changing laser polarizations in order to obtain domain contrast in materials.

Polarization-dependent imaging requires access to both angled and normal incidence in order to enable full access to all selection rules, and the microscope geometry must allow for this. A review of the different instrumental options regarding normal vs angled incidence for PEEM applied to problems in plasmonics can be found in Kahl et al.<sup>34</sup> Whereas angled incidence PEEM is widely common in practice, normal incidence PEEM is less common but enables variation in the alignment of incident laser polarization with a material without changing the in- and out-of-plane components of the electric field, which can have very different photoemission cross sections that could complicate data analysis. Figure 1 shows two PEEM instrumental setups of different geometries: in design (a), PEEM is combined with LEEM mode, and normal incidence illumination is achieved by directing an incident laser beam using a magnetic sector field, whereas in design (b), the incident laser is reflected from a rhodium mirror in the microscope column and

involves electrostatic optics.<sup>34</sup> In both designs, the normal incidence path is highlighted in green in Fig. 1. There are two different ways to conduct normal-incidence polarization-dependent experiments: variation in the photon polarization while keeping the sample alignment static with respect to incoming photons, or vice versa. In practice, changing the photon polarization is usually easier to implement and reduces the need for image registration to extract domain information. However, particularly in the case of synchrotron radiation sources, changing the polarization of x rays can be complicated, and changes are often made to the sample instead.<sup>44</sup>

#### **B. Selection rules in PD-PEEM**

PD-PEEM exploits spatial variation in the orientation of the electronic structure for domain imaging on the nanoscale. The primary working principle of PD-PEEM relies on the fact that the rate of optical transitions between different electronic states is subject to optical selection rules. Therefore, if domains in a material are ordered such that they have different optical selection rules, one can use PD-PEEM to identify domains and their properties. There are three different ways to consider these optical selection rules, as we discuss next; all of them are effectively equivalent but useful to, and appreciated by, the Chemistry and Physics communities differently. Some optical transitions in photoemission are single-photon processes, while others are multi-photon processes. Selection rules govern all photon interactions, and therefore, sometimes multiple selection rules need to be considered simultaneously.

## 1. Spatial variation in transition dipole moment

Fermi's golden rule states that the rate of transition between an initial state  $|i\rangle$  and a final state  $|f\rangle$  is determined by the transition moment integral, which is given by

$$U_{fi} \propto \langle f | \vec{\varepsilon} \cdot \vec{r} | i \rangle \tag{1}$$

under the long-wavelength approximation, where  $\vec{\epsilon}$  is the light polarization. This simplifies under the electric-dipole approximation

$$U_{fi} \propto \vec{\varepsilon} \cdot \langle f | \sum_{j} \vec{r_{j}} | i \rangle = \vec{\varepsilon} \cdot \vec{\mu_{fi}},$$
 (2)

where  $\vec{\mu_h}$  is the transition dipole moment (TDM) between the initial

Therefore, under these approximations, the rate of transition between the initial and final states is maximized when the laser polarization is parallel to  $\vec{\mu_h}$  and minimized when the polarization is perpendicular to  $\vec{\mu_h}$ .

These selection rules are well known in spectroscopy<sup>46</sup> and are employed for imaging material domains with PD-PEEM. When a transition from an occupied state to a state above the vacuum level (photoemission) occurs with two or more photons, the intermediate state can either be a virtual state or a normally unoccupied state [Fig. 2(a)]. When this state is a normally unoccupied state, then the photoemission probability reflects the transition moment integral for both the first and second photoexcitation processes. Typically, the final state is approximated as a free-electron state, and the selection rules for this second transition are less important than for the first transition. Therefore, a spatial variation in the transition moment integral between the initial and intermediate states can

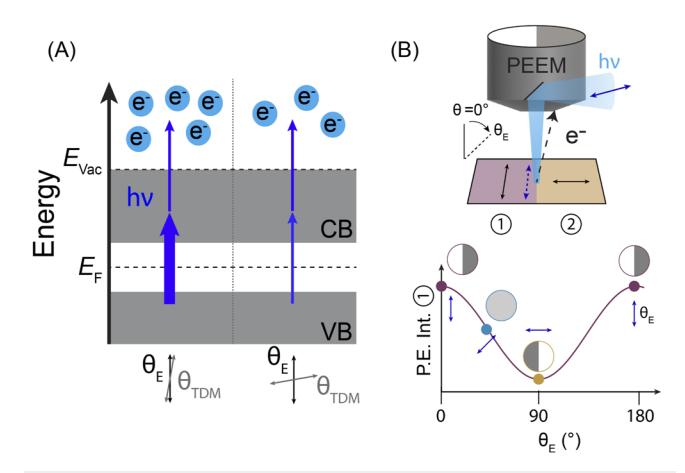


**FIG. 2.** (a) Changing the laser polarization angle  $\theta_{\rm E}$  alignment with the transition dipole  $\theta_{TDM}$  modifies the photon absorption probability, resulting in PEEM imaging contrast. (b) Schematic of PD-PEEM for spatially dependent  $\theta_{TDM}$ . The white shading indicates maximum photoemission intensity, and dark gray indicates minimum intensity. Rotation of  $\theta_{\rm E}$  modulates the photoemission intensity from domains with different atomic displacements and thereby different  $\theta_{\text{TDM}}.$  Reproduced with permission from Spellberg et al., Sci. Adv. 10, eado2136 (2024).<sup>43</sup> Copyright 2024 AAAS Publishing.

provide domain contrast in PD-PEEM, and we can identify the orientation of different domains ( $\theta_{TDM}$ ) by taking PEEM images as a function of laser polarization ( $\theta_E$ ), as shown in Fig. 2(b).

## 2. Spatial variation in dielectric function

The intensity of a transition in PEEM is proportional to the dot product of the laser polarization vector  $\vec{P}$  and the displacement vector  $\vec{D}$ . The displacement vector is the product of the electric field vector  $\vec{E}$  with the tensor for the complex dielectric function of a material,

$$\varepsilon(\omega) = \begin{bmatrix} \varepsilon_{xx}(\omega) & \varepsilon_{xy}(\omega) & \varepsilon_{xz}(\omega) \\ \varepsilon_{yx}(\omega) & \varepsilon_{yy}(\omega) & \varepsilon_{yz}(\omega) \\ \varepsilon_{zx}(\omega) & \varepsilon_{zy}(\omega) & \varepsilon_{zz}(\omega) \end{bmatrix}. \tag{3}$$

Generally, in the case of non-magnetic transitions, only  $\varepsilon_{xx}(\omega)$ ,  $\varepsilon_{yy}(\omega)$ , and  $\varepsilon_{zz}(\omega)$  are non-zero.<sup>47</sup>

Each of the complex dielectric functions  $\varepsilon_{ij}(\omega) = \varepsilon_1^{ij}(\omega)$  $+ \varepsilon_2^{ij}(\omega)i$  can be determined by obtaining the electric polarizability from electronic structure calculations and converting it to the dielectric permittivity.<sup>47</sup> Therefore, the displacement vector will contain information about the symmetries of the initial and final states of an optical transition, and one can then calculate the intensity of the transitions for different laser polarizations. For example, for different laser polarizations that come in normal to a material surface and rotate through the xy plane as shown in Fig. 2(b), the polarization is  $\vec{P} = (\cos \theta, \sin \theta, 0)$  for different angles  $\theta$  in the xy plane.

## 3. Group-theory approaches

Group theory approaches to selection rules are extremely common in molecular spectroscopy but less common for deriving selection rules in solids. However, this approach is exceedingly useful for designing polarization-dependent experiments to uniquely determine domain geometries. An overall review of how to use symmetry rules and group theory approaches for molecular spectroscopy is found in Harris and Bertolucci,48 and here we demonstrate how these approaches can be applied as selection rules for transitions in solids.

While all transition probabilities are dictated by Eq. (1), we can simplify this expression to consider only the symmetries of the initial and final states as well as the symmetry of the laser polarization to determine whether a transition will be allowed. Generally, if the direct product of the irreducible representations for the initial state, final state, and laser polarization contains the totally symmetric irreducible representation of the point group, the transition is an allowed transition. 48 That is to say, if

$$\Gamma(\psi_f) \otimes \Gamma(\varepsilon) \otimes \Gamma(\psi_i)$$
 (4)

contains  $\Gamma(a)$ , where a is the totally symmetric irreducible representation, then the transition is allowed. We shall explain this by using black phosphorus as an example material.

Black phosphorus (BP) is a two-dimensional material with a well-known polarization dependence for its optical transitions. It is part of the base-centered orthorhombic space group Cmca, which has the same symmetries as the  $D_{2h}$  point group. The totally symmetric irreducible representation of this point group is  $\Gamma(A_g)$ , while the wave functions of the conduction band and the valence band near the  $\Gamma$  point of the Brillouin zone can be approximated to have the point groups  $\Gamma_{VB}(B_{2g})$  and  $\Gamma_{CB}(B_{1u})$ . Linear laser polarizations x, y, and z belong to the  $\Gamma(B_{3u})$ ,  $\Gamma(B_{2u})$ , and  $\Gamma(B_{1u})$  point groups, respectively. Therefore, if we calculate the direct products for the conduction and valence band point groups with each of the laser polarizations,

$$\Gamma_{\rm CB}(B_{1u}) \otimes \Gamma_{\rm x}(B_{3u}) \otimes \Gamma_{\rm VB}(B_{2g}) = \Gamma(A_g),$$
 (5)

$$\Gamma_{CB}(B_{1u}) \otimes \Gamma_{y}(B_{2u}) \otimes \Gamma_{VB}(B_{2g}) = \Gamma(B_{1g}),$$
 (6)

$$\Gamma_{\rm CB}(B_{1u}) \otimes \Gamma_{\rm z}(B_{1u}) \otimes \Gamma_{\rm VB}(B_{2g}) = \Gamma(B_{2g}),$$
 (7)

we find that the direct product with the point group belonging to a laser beam polarized along the x direction is the only one to contain the totally symmetric point group  $\Gamma(A_g)$ , and therefore, this is the only allowed transition, meaning that black phosphorus preferentially absorbs light polarized along the x direction (armchair) for the lowest energy across bandgap transitions, as is observed experimentally.50

This analysis, based on a molecular orbital approach, is clearly simplistic compared to the electronic structure calculations required to fully explain transitions in solid state systems. As a first approximation, however, this approach is extremely effective at making qualitative predictions and building intuitive insight. As discussed further in Sec. III D, such analysis is also valid when considering the selection rules for photoemission from magnetic materials.

## III. APPLICATIONS OF PD-PEEM TO DIFFERENT KINDS OF DOMAINS

## A. Molecular and polymer domains

Controlling the morphology of organic electronic films is an enormous area of research. The kind of molecular packing that occurs in films, the degree of order, and the electronic structure of polycrystalline grain boundaries all impact the functionality of these films. The size of crystalline domains and the relative orientation of molecular components have been shown to impact charge carrier mobility in hybrid electronic materials.<sup>51</sup> Currently, many experimental efforts to characterize and investigate these kinds of films use a wide suite of techniques to investigate the role of molecular and polymer domains in functionality.<sup>51</sup> <sup>52</sup> While this can be an effective approach, comparisons between molecular and polymer order and excited state dynamics all in the same experimental apparatus would be highly valuable for disentangling the complex role of morphology in molecular and polymer films. PD-PEEM is, therefore, a powerful tool for investigating and characterizing molecular and polymer materials. In both ordered and semi-ordered films, PD-PEEM can provide information regarding the spatial variation in the

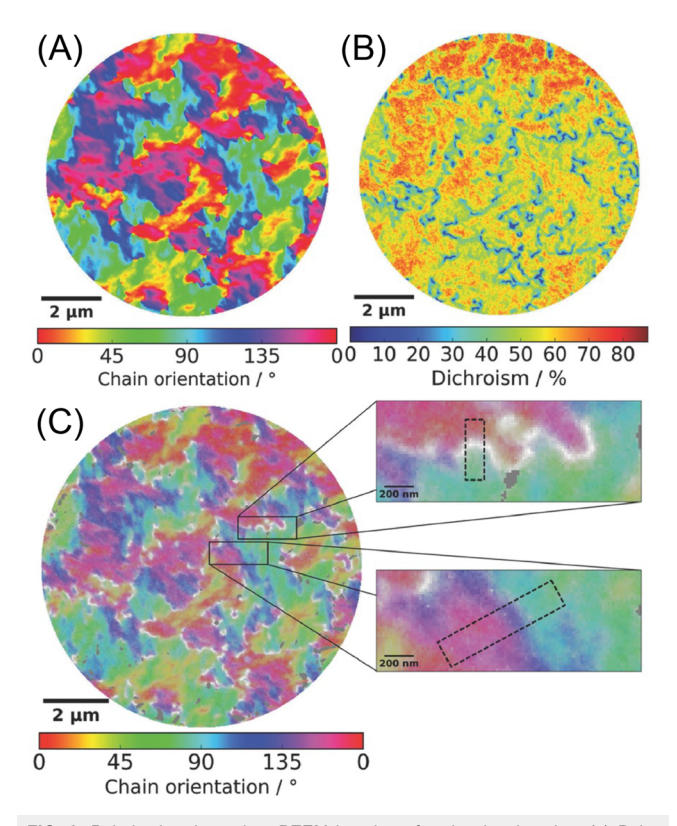


**FIG. 3.** Polarization-dependent PEEM imaging of molecular domains. (a) Polymer orientation map of P3HT spin-coated onto silicon with native oxide imaged at 400 nm. (b) Degree of dichroism for the same regions in (a) and (c) a composite figure that shows both polymer orientation and then opacity based on the degree of dichroism. The insets show the high spatial resolution that can be achieved with this approach. Reproduced with permission from Neff *et al.*, Adv. Mater. **29**, 1701012 (2017). Copyright 2017 Wiley Publishing.

direction of the in-plane transition dipole moment and variations in the strength of the polarization anisotropy for molecular materials. One of the first instances where PD-PEEM was employed to probe material heterogeneity in molecular systems was investigating polymer crystallinity and orientation. Figures 3(a)–3(c) show the results of a PD-PEEM experiment investigating P3HT that has been spin-coated on a Si/SiO2 surface. P3HT is a semiconducting polymer with a transition dipole moment that lies along the polymer backbone. Depending on the preparation conditions, the polymer will crystallize into domains of different sizes and degrees of disorder. The size of crystalline domains and the degree of polymer crystallinity can be readily observed in PD-PEEM by fitting the photoemission response as a function of the laser polarization  $\theta_E$  to

$$I_{\text{PE}}(\theta) = A\cos^2(\theta_{\text{E}} - \theta_{\text{TDM}}) + C,$$
 (8)

where A is the modulation amplitude and C is the photoemission baseline. Plotting  $\theta_{\text{TDM}}$  [Fig. 3(a)] with respect to position on the sample surface reveals the local orientation of the polymers. The strength of the polarization dependence depends on the degree of order of the polymer chains [Fig. 3(b)] and is quantified by the photoemission dichroism,

$$\rho = \frac{I_{\text{max}} - I_{\text{min}}}{I_{\text{max}} + I_{\text{min}}} = \frac{A}{A + 2C}.$$
 (9)

Combining these two values in a composite image shows the correlation between how abruptly the polymers change orientations between adjacent domains and the degree of order at their boundaries [Fig. 3(c)]. This work has been extended to investigating other aspects of polymer growth and deposition, analyzing the persistence length of polymers under different conditions such as preparation methods, co-deposition, and temperature. Length of materials are using PD-PEEM to analyze this class of materials and we anticipate that such utilization of this technique will only grow as it becomes more widely established.

## B. Local symmetry variation in 2D materials

Just as molecular materials can have variations in nanoscale morphology that impact their properties, inorganic materials can vary on the nanoscale. Such morphology variation does not always consist of regions of structural or spin alignment, such as the ferroelectric or magnetic domains discussed in Secs. III C and III D, but instead consists of local variations in electronic structure symmetry due to morphology, such as edges. There are multiple experimental techniques that can be used to access this kind of information, but PD-PEEM has a different approach than many. Rather than imaging variations in the electronic structure on the nanoscale, PD-PEEM accesses variations in the *symmetry* of electronic states on the nanoscale.

Figure 4(a) shows a PD-PEEM local transition dipole map of 2D BP. BP is birefringent, preferentially absorbing light that is polarized along the armchair direction of its corrugated orthorhombic crystal structure. This polarization dependence is due to the symmetry of the electronic transitions, such as transition (2) shown in Figs. 4(b) and 4(d) and discussed in Sec. II B. However, the edges of BP have electronic states with transition dipole moments that are

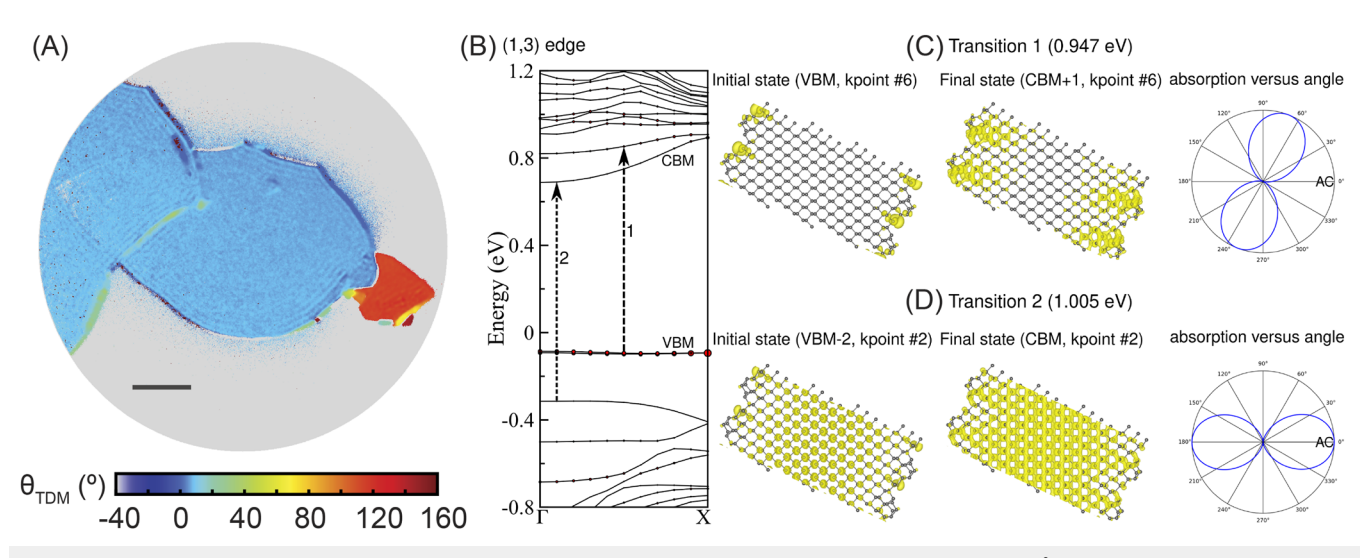


**FIG. 4.** (a)  $\theta_{TDM}$  map of two-dimensional black phosphorus taken with 2.4 eV photons. The map is median-filtered with a  $3 \times 3$  pixel<sup>2</sup> neighborhood, and only pixels with an  $R^2 > 0.6$  are shown. Scale bar:  $5 \mu m$ . (b) Electronic band structure of a monolayer BP nanoribbon with a (1,3) edge with the valence band maximum (VBM) and conduction band minimum (CBM) labeled, where the Fermi level is energy = 0 eV. The red circles superimposed on the bands correspond to the contribution from the edge atoms. For two representative optical transitions (indicated by the arrows), spatial distributions of the charge densities of the initial and final states and polarization-angle-dependent absorption profiles are shown in (c) and (d). Reproduced with permission from Joshi *et al.*, Nano Lett. **22**, 3180 (2022).<sup>53</sup> Copyright 2022 ACS Publications.

influenced both by the electronic state transitions of the crystal interiors but also by the symmetries of the edges and edge electronic states, such as transition (1) shown in Figs. 4(b) and 4(c). These kinds of edge electronic states have subsequently been observed with PL microscopy.<sup>59</sup> This methodology is not unique to black phosphorus; there are numerous other anisotropic materials where variations in local electronic structure and symmetry could result in contrast in PD-PEEM. We anticipate tin selenide<sup>60</sup> and molybdenum trioxide<sup>61</sup> as suitable material candidates for such a study.

## C. (Anti)ferroelectricity

Ferroelectric materials are those containing a reversible spontaneous electric polarization. This polarization arises from a shift in atomic positions relative to a symmetric paraelectric phase that exists at higher temperatures. When groups of adjacent unit cells contain atomic displacements in the same direction, they form a ferroelectric domain, a nano- to micrometer-scale region with a singular polarization direction.4 This property can be measured electrostatically<sup>62</sup> or mechanically by piezoforce response.<sup>63</sup> These materials, however, typically contain a complex arrangement of differently oriented domains. Implementation of ferroelectric materials in device applications requires knowledge and control over the domain structure. As such, a number of methods have been developed for imaging ferroelectric domains to spatially resolve and measure polarization directions. These include STM, <sup>64,65</sup> STEM, <sup>66</sup> PFM,63 polarized light microscopy (PLM),67 and PEEM.68 Work function contrast has been used for resolving out-of-plane (OOP) domains with PEEM due to the different surface charge densities that form depending on whether the polarization direction points up or down,68 but it cannot be used to determine in-plane (IP) polarization directions. Rather, to access IP domains, PD-PEEM is used. The ferroelectric lattice distortion creates anisotropy in the electronic structure, such that the photoemission intensity is dependent on the light polarization orientation. This can manifest in core electronic states as well as in the valence and conduction bands and is accessible by probing the material with the relevant excitation energy for the desired electronic transition. <sup>58,69</sup>

Lead zirconate titanate (PZT) is a commonly used ferroelectric material in both device applications and basic research. It exhibits both IP and OOP ferroelectric domains whose arrangement is readily controllable via external biasing. 10 These structural distortions impact the symmetry of the Ti core levels, such that there is a significant x-ray linear dichroism in the Ti L edge. Therefore, by measuring the total electron yield with respect to rotating the xray polarization, the different domains can be separately resolved.<sup>58</sup> The photoemission signal is dependent on the projection of the polarization direction onto the light's electric field vector, so by illuminating at angled incidence, both IP and OOP domains are measured. Figure 5(a) schematically shows the experiments, and Fig. 5(b) shows an XPEEM image at the indicated polarization angles. As the polarization axis rotates relative to the three directions, different domains appear bright and dark. Integrating the photoemission intensity in each domain with respect to x-ray polarization reveals a cos<sup>2</sup> dependence, where maximum photoemission occurs when the x-ray polarization is perpendicular to the ferroelectric polarization axis.<sup>58</sup> In other words, the TDM is oriented orthogonal to the direction of atomic displacement. This is not strictly the case for all ferroelectric materials but will depend on the specific structure and transition being accessed. Without a second probe to determine crystalline axes, PD-PEEM can determine relative orientations between domains and accurately determine optical axes with respect to the lab coordinate frame but not with respect to

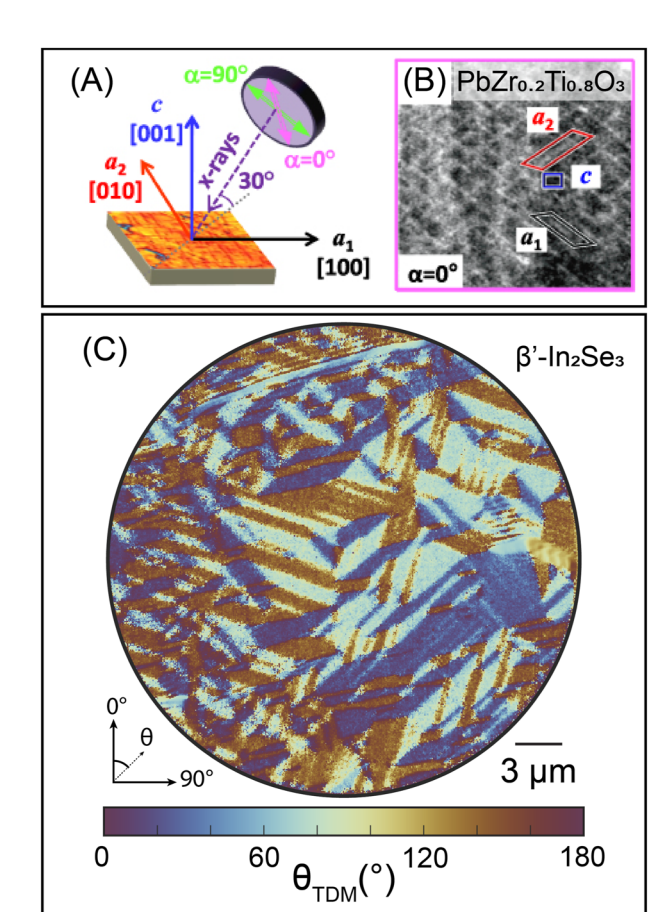


FIG. 5. (a) Schematic of a polarization dependent XPEEM experiment on PZT with lattice vectors and x-ray axes indicated. (b) Divided dichroic PEEM image taken at the shoulder of the Ti L3A-edge with x-ray polarization axis  $\alpha = 0^{\circ}$ . (c) Map of the  $\theta_{\text{TDM}}$  parameter fit to each pixel in the PD-PEEM data to reveal antiferroelectric domains in  $\beta'$ -ln<sub>2</sub>Se<sub>3</sub>. The color bar<sup>56,57</sup> shows three distinct domains resolved as blue, cyan, and brown. (a) and (b) Reproduced with permission from Polisetty et al., J. Phys. Condens. Matter 24, 245902 (2012).58 Copyright 2012 IOP Publishing. (C) Reproduced with permission from Spellberg et al., Sci. Adv. 10, eado2136 (2024).43 Copyright 2024 AAAS Publishing.

lattice directions. 43 In addition, for materials with polarization directions at arbitrary orientations in 3D space or multiferroics containing multiple order parameters with separate polarization responses, domain arrangements can still be imaged with PD-PEEM, but complementary methods are required to extract unique ferroelectric polarization directions for each domain.

Because PD-PEEM is sensitive to the material's electronic structure, a net lattice polarization is not necessarily required for domain contrast to be observed. In antiferroelectric materials, for example, unit cells contain equal and opposite atomic distortions such that there is zero net polarization. The electronic structure orientation, however, is controlled by the antiferroelectric domain structure and is, therefore, readily accessible via PD-PEEM.  $\beta'$ -In<sub>2</sub>Se<sub>3</sub> is one such material, as it contains IP antiferroelectric distortions that occur in any of three equivalent directions.<sup>26</sup> As such, three domain variants are possible and can be imaged with near-normal incidence PD-PEEM, where different regions of  $\beta'$ -In<sub>2</sub>Se<sub>3</sub> are brighter or darker depending on the local alignment between  $\theta_{\text{TDM}}$  and  $\theta_{E}$ , corresponding to the rotated lattice between domains.<sup>43</sup> Figure 5(c) shows a map of  $\theta_{TDM}$  for a  $\beta'$ -In<sub>2</sub>Se<sub>3</sub>, where predominantly three domain orientations are observed due to the threefold symmetry of the parent structure. As in the case of XPEEM imaging of PZT, an external probe of lattice directions is required to correlate  $\theta_{TDM}$  measured by PD-PEEM to the direction of atomic displacements because the orientation of  $\theta_{TDM}$  depends on the excitation energy.<sup>43</sup> Nevertheless, PD-PEEM remains a powerful technique for the study of (anti)ferroelectric materials as it reveals arrangements of domains across regions of tens of micrometers while maintaining high resolution and orientational precision.

## D. Ferromagnetism

The emerging class of 2D van der Waals magnetic materials holds enormous potential for applications in spintronics devices due to tunable electronic states as well as existing magnetic orders that allow spin manipulation. 73-75 In particular, imaging magnetic domain formation in such 2D materials could significantly contribute toward the understanding of 2D magnetism. <sup>16</sup> When considering ferromagnetic materials, a straightforward method for domain imaging without the complication of adding a spin analyzer is utilizing magnetic circular dichroism (MCD),<sup>47</sup> which is given by the differential absorption/reflection of left and right circularly polarized light induced in a material in the presence of a magnetization oriented parallel to the light propagation direction. In ferromagnets, MCD is caused by the intrinsic exchange interaction and spin-orbit interaction (SOI). For the past few decades, x-ray magnetic circular dichroism (XMCD) PEEM has been the most popular technique to image magnetic domains since x rays have access to the core-shell electrons where the SOI is large and, hence, the spin-split transitions are simple to interpret. 5,76,77 In addition, XMCD PEEM image contrast is given by the projection of the magnetic moments along the incident x-ray beam direction, thereby enabling the construction of magnetization vector mapping for a magnetized material. Although XMCD PEEM is a powerful tool for investigating magnetic order in ferromagnets, it demands access to sophisticated synchrotron facilities. Therefore, a table-top experimental technique employing light sources with UV and visible frequencies is valuable that can facilitate magnetic domain imaging. Whereas magneto-optical Kerr effect (MOKE) microscopy and other light based techniques<sup>78</sup> involve a rather straightforward experimental setup for studying magnetism with optical frequency, the associated spatial resolution is limited by the diffraction limit of light. These challenges can be overcome by employing threshold PEEM, which, unlike x-ray PEEM, uses optical frequencies with photon energies near the work function of a material to probe the valence shell electrons. In 3d ferromagnetic transition metals, the SOI in the valence bands is much weaker than the core shells. The exchange splitting, however, can be large in certain materials for the bands near the Fermi level  $(E_F)$ , resulting in large MCD and even magnetic linear dichroism (MLD) in valence band photoemission. Using UV photons, Nakagawa and Yokoyama<sup>79</sup> and Hild et al.<sup>80</sup> reported such threshold photoemission (TP) MCD in out-of-plane magnetized Ni/Cu(100) and Co/Pt(111) through 1PPE PEEM. We would like to emphasize that since both TP MCD PEEM and MLD PEEM image contrasts are

obtained by tuning the incident laser polarization, whether circular or linear, both of these techniques can be classified as PD-PEEM.

In TP MCD, the major asymmetry contribution emerges from the UV photon absorption process, as illustrated in Fig. 6(a) for SrTiO<sub>3</sub> when illuminated by a laser with photon energy of 4.66 eV.<sup>71</sup> The initial spin-polarized states, i.e., the spin split states caused by the exchange interaction originating from the magnetization near  $E_F$ , play a pivotal role in this process. In other words, the energy separation of the spin-polarized initial states is a measure of the MCD asymmetry in threshold PEEM because the helicity of the incident circularly polarized photons couples to the spin of the electrons via spin-orbit coupling. The schematic in Fig. 6(b) demonstrates the mechanism of such helicity selective TP PEEM imaging of magnetic domains with out-of-plane magnetization; an example of TP MCD PEEM imaging of magnetic domains of SrTiO<sub>3</sub> is shown in Figs. 6(c) and 6(d), studied by Taniuchi et al.71 In an earlier study, Kronseder et al.72 reported such domain imaging TP MCD PEEM imaging in fcc-Ni(100) [Figs. 6(e)-6(h)]. Figure 6(e) shows the calculated spin polarization (difference of minority and majority electrons) of bands near  $E_F$  for fcc-Ni(100), which reveals a reversal of spin polarization

between 0.2 and 0.4 eV below  $E_F$ . Consequentially, circularly polarized light of opposite helicities with energy near  $E_F$  selectively excites electrons from these spin-polarized states above the vacuum level to be detected by PEEM imaging. This is evident from the magnetic contrast in Fig. 6(f) that shows the PEEM images of the Cs deposited 16 ML Ni/Cu(100) surface when illuminated by 405 nm right circularly polarized light incident at an angle of 65° with respect to the surface normal. Identical to XMCD PEEM, TP MCD PEEM image contrast is given by  $\mathbf{M} \cdot \mathbf{h}$ , where  $\mathbf{M}$  denotes the magnetization direction in a domain (out-of-plane and into-plane) and h denotes the helicity of the incident light, which is aligned in a parallel/antiparallel direction with M. The TP MCD asymmetry from the recorded PEEM image of Ni/Cu(100) in Fig. 6(f) is shown in Fig. 6(g) [and Fig. 6(h) for a magnified region]. Notably, in addition to MCD, MLD has also been detected using the threshold PEEM technique for a polycrystalline Fe film with in-plane magnetization, resulting in 0.37% asymmetry.81 It has also been established that group theory and symmetry arguments can be utilized to choose the appropriate geometry for the PEEM experimental setup to determine the presence of MCD and MLD in magnetic materials.8

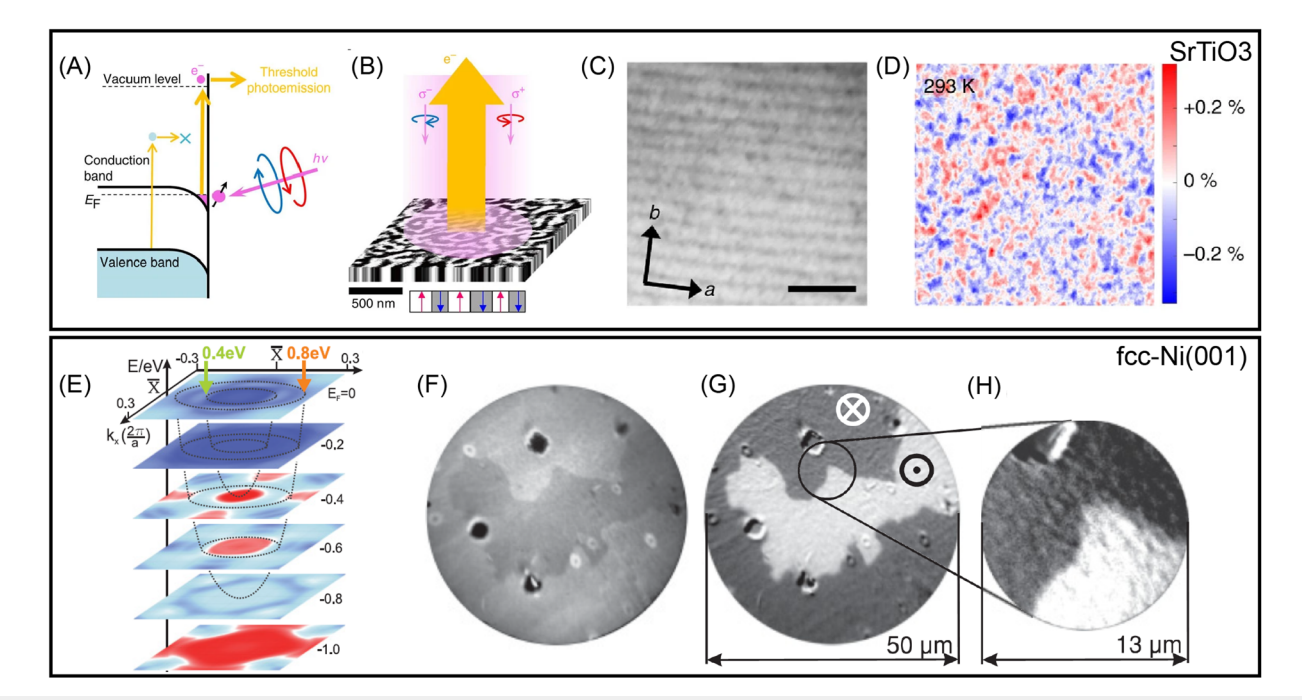


**FIG. 6.** (a) Excitation process of threshold photoemission at the surface of  $SrTiO_3$ . Circularly polarized photons are irradiated on the sample surface, and the spin polarization of the ejected photoelectrons is detected. (b) The magnetic image in the illustration shows a magnetic domain structure in a FePt epitaxial thin film with perpendicular magnetic anisotropy as a typical example. The field of view is 2  $\mu$ m. (c) Raw laser-PEEM image of  $SrTiO_3$  after annealing at 1000 K. (d) Magnetic image at room temperature in the same position as the raw image. Red and blue indicate positive and negative MCD signals, respectively, which correspond to perpendicular magnetization with spin-up and spin-down. The scale bar indicates 500 nm. (e) The LSDA + DMFT spin polarization (minority minus majority electrons) of the surface-projected Bloch spectral function of out-of-plane magnetized fcc-Ni(001) is shown for different energies below the Fermi level  $E_F$ . Blue means more minority electrons, and red means more majority electrons.

Due to the energy–wave-vector relation in the free-electron approximation  $E = \frac{f^2 k_\perp^2}{2m}$ , the available initial  $k_i$  vectors of the photoemission process are within a paraboloid, schematically shown in (e) for 0.4 eV (green) and 0.8 eV (orange). (f) PEEM image taken with *right circularly polarized* light (405 nm). (g) TP-MCD image. (h) Zoomed-in image. (a)–(d) Reproduced with permission from Taniuchi *et al.*, Nat. Commun. 7, 11781 (2016).<sup>71</sup> Copyright 2016 Springer Nature Publishing. (e)–(h) Reproduced with permission from Kronseder *et al.*, Phys. Rev. B 83, 132404 (2011).<sup>72</sup> Copyright 2011 APS Publishing.

The above discussion and recent research 71,84,85 certainly establish TP MCD PEEM, or in a generalized term PD-PEEM, as a promising tool in imaging and characterizing domains in ferromagnets. Furthermore, because XMCD PEEM has been extremely successful in investigating magnetic domain properties in 2D ferromagnets, 16,86,87 we expect that TP MCD PEEM has strong potential to emerge as a suitable tool for investigating the surface properties of 2D van der Waals magnets.

#### **IV. CHALLENGES WITH PEEM**

While PEEM provides a number of notable advantages improved spatial resolution and better ability to discriminate between spatial domains—it has some notable challenges, the biggest ones being the sample requirements and space charging. While differentially pumped "ambient-pressure" PEEM instruments do exist, they are not currently employed in PD-PEEM and do not relax the vacuum requirements of PEEM all the way to atmospheric pressure. This means that samples for PD-PEEM must be ultrahigh vacuum compatible. In addition, because the sample surface forms part of the imaging system, variations in surface roughness impact the electric fields of the objective lens, so samples must be flat to obtain optimal spatial resolution. Notably, we have found that there is flexibility in samples within these constraints, much more so than the prevailing wisdom has suggested. Using PEEM, we have successfully imaged drop-cast 2D materials,<sup>97</sup> biological materials encapsulated in resin,89,9 <sup>0</sup> and hundreds of nanometers thick van der Waals materials.43

The other major challenge with using PEEM is space-charging and how it can impact spatial resolution and signal to noise. PEEM is an electron imaging technique, which means that, similar to SEM and TEM, if too many electrons are interacting with a sample, or are at the same location in an electron lens at the same time, they will interact with each other and cause a blurring of the image. Therefore, for the optimal spatial resolution, one needs to operate as close to the single-electron emission limit as possible. There are a few different ways to achieve this: through the use of CW light sources, such as Hg and He lamps; bright x-ray sources, such as synchrotrons; or high repetition-rate (few to tens of MHz) pulsed laser sources. Each of these options has associated benefits and limitations. For CW and x-ray sources, control of polarization can be challenging, but pulsed laser sources have lower signal counts. However, pulsed laser sources have a limit to the k-space regions that can be accessible for photoemission depending on their photon energy and are most affected by space charging because photon flux (and, thus, electron emission) is concentrated within pulses. Pulsed laser sources provide other benefits, such as the ability to conduct two-photon PD-PEEM, which is what has been used for many of the experiments described above and can be easily extended for combining time-resolved experiments with measurements of material domains.

#### V. NEW DIRECTIONS

Polarization-dependent PEEM is a comparatively new method for investigating domain formation in materials. With its nanoscale

spatial resolution, photon-based material interrogation, and wide field of view of tens of  $\mu$ m, it occupies a unique space in the landscape of imaging methods. The benefits of photon-interrogation, including control of laser pulse duration, energy, and polarization, enable wide flexibility in experimental design that we believe will be critical for investigating the domains, properties, and dynamics of nanoscale materials. In particular, it is the ability to probe different kinds of domain formation in materials with the same instrument that makes PEEM an intriguing possibility for investigating multiferroic

Multiferroic materials contain both electric dipole and spin ordering that can be controlled by electric and magnetic fields.<sup>6</sup> There are numerous fundamental scientific questions in multiferroics, with correlated degrees of freedom, that could be investigated with PD-PEEM regarding domain formation and melting over phase boundaries. Figure 7 shows different techniques, including PD-PEEM, which have successfully imaged domains in the multiferroic BiFeO<sub>3</sub>. Depending on whether BiFeO<sub>3</sub> is grown epitaxially<sup>70</sup> or as single crystals, <sup>69,88</sup> there is a difference in whether ferroelectric and antiferromagnetic order are correlated. The relationship between sample strain, growth methods, and correlated order is an open question in BiFeO<sub>3</sub> that could be probed comprehensively with PD-PEEM. However, equally challenging is how the insight from the different techniques in Fig. 7 can be combined: (i) PFM in (a), which images in-plane ferroelectric domains with four different types of orientations; (ii) XPEEM in (b), which is able to selectively image ferroelectric domains of a specific orientation and obtain insights into associated magnetic order; (iii) STEM in (c) and (d), which captures ferroelectric domain walls along with polarization mapping in sub-nm resolution; (iv) PLM in (e), which uses ferroelectricity induced birefringence for domain imaging; and (v) linear and circular PD-PEEM in (f) and (g), which shows domains (1, 3, and 4) with different contrast in LD PEEM (f) that have identical contrast with PLM (e). Further work is required to employ PD-PEEM for efficiently and sensitively detecting the contributions of electric and magnetic order simultaneously in multiferroics and to interpret how the insights of PD-PEEM can be combined with other methods.

Similarly, there are untapped opportunities for exploring ferroic materials<sup>92,93</sup> and interactions with polycrystalline molecular and polymer layers<sup>94</sup> for controlling switchable domain behavior in materials that are critical for applications in computing, memory, and next generation devices, such as memory-on-chip and neuromorphic computing architectures. 95,96 PD-PEEM provides an opportunity to understand how light, strain, electric field, thickness, and molecular modification can be used to control and modify domain behavior. Manipulating the domain properties of solid state materials by tuning all these parameters and characterizing their properties using PD-PEEM is, therefore, an open question for future research directions.

Finally, as an emerging technique for domain imaging, it is essential to connect the interpretation of physical observables measured with PD-PEEM with domain imaging obtained from more established methods, as has been mentioned in Secs. I, III C, and III D and shown in Fig. 7. We anticipate that combining PEEM with other more established techniques will contribute remarkably toward a comprehensive understanding of solid state materials.

Given the flexibility of domains that can be imaged with PD-PEEM, the opportunities for using this technique for investigating

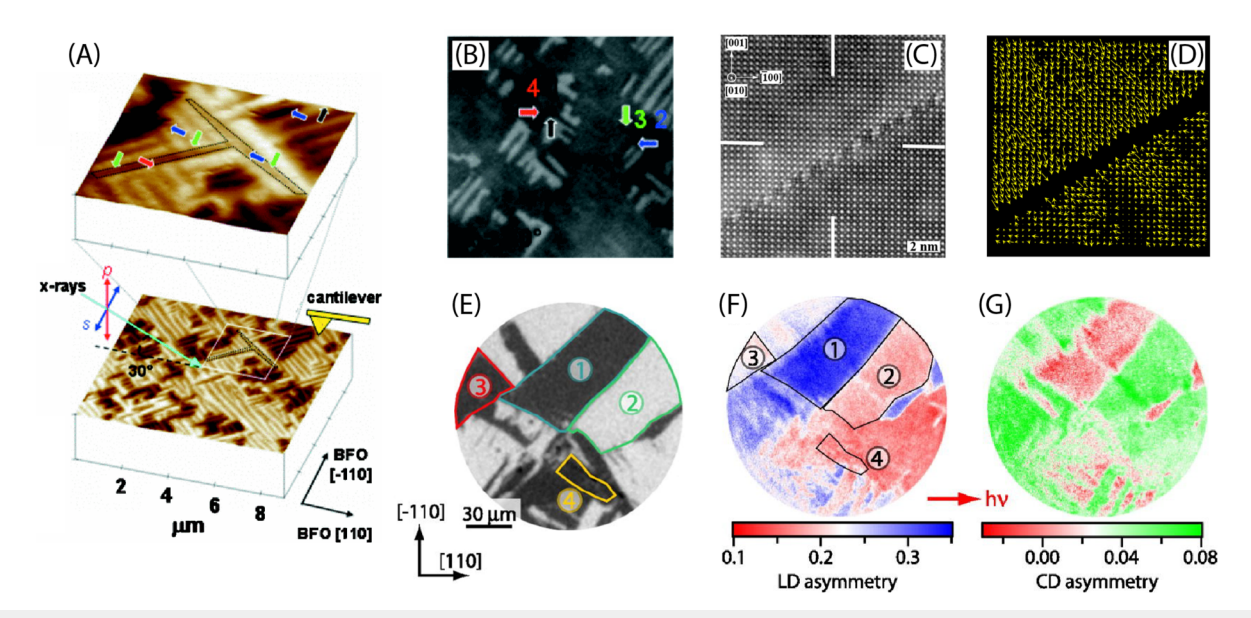


FIG. 7. Various methods for imaging domains in multiferroic BiFeO<sub>3</sub>. (a) In-plane PFM and (b) XPEEM images of the same region of cross-hatch domains. (c) Annular dark-field STEM image of the domain boundary and (d) two-dimensional vector plot of atomic displacements (yellow arrows) to indicate the polarization direction in each domain. (e) Polarized light microscopy, (f) threshold PEEM linear dichroism, and (g) circular dichroism images of the same region. (a) and (b) Reproduced with permission from Holcomb *et al.*, Phys. Rev. B **81**, 134406 (2010). Copyright 2010 APS Publishing. (c) and (d) Reproduced with permission from Ge *et al.*, Microstructures **3**, 2023026 (2023). Copyright 2023 OAE Publishing. (e)–(g) Reproduced with permission from Sander *et al.*, J. Appl. Phys. **118**, 224102 (2015). Copyright 2015 AIP Publishing.

heterogeneity, domain formation, and modulation in materials are vast, and the future for PD-PEEM is bright.

#### **ACKNOWLEDGMENTS**

The authors thank Dr. Prakriti P. Joshi for early discussions regarding the Perspective and her suggestions during editing. This work was funded by the Office of Basic Energy Sciences, U.S. Department of Energy (Grant No. DE-SC0021950). A.G. acknowledges the support from a Kadanoff-Rice Postdoctoral Fellowship funded by the University of Chicago Materials Research and Engineering Center supported by the National Science Foundation under Award No. DMR-2011854.

## **AUTHOR DECLARATIONS**

#### **Conflict of Interest**

The authors have no conflicts to disclose.

## **Author Contributions**

Atreyie Ghosh: Data curation (equal); Writing – original draft (equal); Writing – review & editing (equal). Joseph L. Spellberg: Data curation (equal); Writing – original draft (equal); Writing – review & editing (equal). Sarah B. King: Conceptualization (lead); Funding acquisition (lead); Supervision (lead); Writing – original draft (lead); Writing – review & editing (equal).

## **DATA AVAILABILITY**

Some of the data referenced in this paper are openly available in Zenodo at the following DOIs and references: http://doi.org/10.5281/zenodo.6407182, from Joshi *et al.*,<sup>53</sup> and https://doi.org/10.5281/zenodo.10994899, from Spellberg *et al.*<sup>43</sup>

## REFERENCES

- <sup>1</sup>R. Noriega, J. Rivnay, K. Vandewal, F. P. V. Koch, N. Stingelin, P. Smith, M. F. Toney, and A. Salleo, Nat. Mater. **12**, 1038 (2013).
- <sup>2</sup> A. Neff, F. Niefind, B. Abel, S. C. B. Mannsfeld, and K. R. Siefermann, Adv. Mater. **29**, 1701012 (2017).
- <sup>3</sup>K. Lu, Nat. Rev. Mater. 1, 16019 (2016).
- <sup>4</sup> A. K. Tagantsev, L. E. Cross, and J. Fousek, *Domains in Ferroic Crystals and Thin Films* (Springer, New York, 2010).
- <sup>5</sup>C. M. Schneider and G. Schnhense, Rep. Prog. Phys. 65, 1785 (2002).
- <sup>6</sup>J. Rivnay, L. H. Jimison, J. E. Northrup, M. F. Toney, R. Noriega, S. Lu, T. J. Marks, A. Facchetti, and A. Salleo, Nat. Mater. **8**, 952–958 (2009).
- <sup>7</sup>S. S. Cheema, N. Shanker, S.-L. Hsu, J. Schaadt, N. M. Ellis, M. Cook, R. Rastogi, R. C. N. Pilawa-Podgurski, J. Ciston, M. Mohamed, and S. Salahuddin, Nature **629**, 803 (2024).
- <sup>8</sup>Y. Cho, K. Fujimoto, Y. Hiranaga, Y. Wagatsuma, A. Onoe, K. Terabe, and K. Kitamura, Appl. Phys. Lett. **81**, 4401 (2002).
- <sup>9</sup> A. V. Ievlev and S. V. Kalinin, Nanoscale 7, 11040 (2015).
- <sup>10</sup>F. Risch, Y. Tikhonov, I. Lukyanchuk, A. M. Ionescu, and I. Stolichnov, Nat. Commun. 13, 7239 (2022).
- <sup>11</sup>P. D. Lomenzo, S. Li, B. Xu, T. Mikolajick, and U. Schroeder, IEEE Sens. J. 24, 12050 (2024).
- <sup>12</sup>S. Wan, Q. Peng, Z. Wu, and Y. Zhou, ACS Appl. Mater. Interfaces 14, 25693 (2022).

- <sup>13</sup> M. E. Ziebel, M. L. Feuer, J. Cox, X. Zhu, C. R. Dean, and X. Roy, Nano Lett. **24**, 4319 (2024).
- <sup>14</sup>E. Meirzadeh, I. Azuri, Y. Qi, D. Ehre, A. M. Rappe, M. Lahav, L. Kronik, and I. Lubomirsky, Nat. Commun. 7, 13351 (2016).
- <sup>15</sup>H. Tanaka, A. Wakamatsu, M. Kondo, S. Kawamura, S.-i. Kuroda, Y. Shimoi, W.-T. Park, Y.-Y. Noh, and T. Takenobu, Commun. Phys. 2, 96 (2019).
- <sup>16</sup>Q. Li, M. Yang, C. Gong, R. V. Chopdekar, A. T. N'Diaye, J. Turner, G. Chen, A. Scholl, P. Shafer, E. Arenholz, A. K. Schmid, S. Wang, K. Liu, N. Gao, A. S. Admasu, S.-W. Cheong, C. Hwang, J. Li, F. Wang, X. Zhang, and Z. Qiu, Nano Lett. 18, 5974 (2018).
- <sup>17</sup> M. Giraldo, Q. N. Meier, A. Bortis, D. Nowak, N. A. Spaldin, M. Fiebig, M. C. Weber, and T. Lottermoser, Nat. Commun. 12, 3093 (2021).
- <sup>18</sup> H. J. Kim, J. W. Kim, H. H. Lee, T.-M. Kim, J. Jang, and J.-J. Kim, J. Phys. Chem. Lett. 2, 1710 (2011).
- <sup>19</sup>S. Nishikata, G. Sazaki, J. T. Sadowski, A. Al-Mahboob, T. Nishihara, Y. Fujikawa, S. Suto, T. Sakurai, and K. Nakajima, Phys. Rev. B 76, 165424 (2007).
- <sup>20</sup>L. V. de Groot, K. Fabian, I. A. Bakelaar, and M. J. Dekkers, Nat. Commun. 5, 4548 (2014).
- <sup>21</sup> C. Cui, W.-J. Hu, X. Yan, C. Addiego, W. Gao, Y. Wang, Z. Wang, L. Li, Y. Cheng, P. Li, X. Zhang, H. N. Alshareef, T. Wu, W. Zhu, X. Pan, and L.-J. Li, Nano Lett. 18, 1253 (2018).
- <sup>22</sup>J. M. Atkin, S. Berweger, A. C. Jones, and M. B. Raschke, Adv. Phys. **61**, 745–842 (2012).
- <sup>23</sup> A. A. Govyadinov, S. Mastel, F. Golmar, A. Chuvilin, P. S. Carney, and R. Hillenbrand, ACS Nano 8, 6911 (2014).
- <sup>24</sup>F. G. Kaps, S. C. Kehr, and L. M. Eng, arXiv.2308.06023 (2023).
- <sup>25</sup> A. Gruverman, M. Alexe, and D. Meier, Nat. Commun. **10**, 1661 (2019).
- <sup>26</sup>C. Xu, J. Mao, X. Guo, S. Yan, Y. Chen, T. W. Lo, C. Chen, D. Lei, X. Luo, J. Hao, C. Zheng, and Y. Zhu, Nat. Commun. 12, 3665 (2021).
- <sup>27</sup>S.-W. Cheong, M. Fiebig, W. Wu, L. Chapon, and V. Kiryukhin, npj Quantum Mater. 5, 3 (2020).
- <sup>28</sup>G. Nordahl and M. Nord, Microsc. Microanal. **29**, 574 (2023).
- <sup>29</sup> E. Gati, Y. Inagaki, T. Kong, R. J. Cava, Y. Furukawa, P. C. Canfield, and S. L. Bud'ko, Phys. Rev. B **100**, 094408 (2019).
- <sup>30</sup> M. Ilett, M. S'ari, H. Freeman, Z. Aslam, N. Koniuch, M. Afzali, J. Cattle, R. Hooley, T. Roncal-Herrero, S. M. Collins, N. Hondow, A. Brown, and R. Brydson, Philos. Trans. R. Soc., A 378, 20190601 (2020).
- <sup>31</sup> P. Schädlich, F. Speck, C. Bouhafs, N. Mishra, S. Forti, C. Coletti, and T. Seyller, Adv. Mater. Interfaces **8**, 2002025 (2021).
- <sup>32</sup>C. Zheng, L. Yu, L. Zhu, J. L. Collins, D. Kim, Y. Lou, C. Xu, M. Li, Z. Wei, Y. Zhang, M. T. Edmonds, S. Li, J. Seidel, Y. Zhu, J. Z. Liu, W.-X. Tang, and M. S. Fuhrer, Sci. Adv. 4, eaar7720 (2018).
- <sup>33</sup> M. J. Prieto and T. Schmidt, Catal. Lett. **147**, 2487 (2017).
- <sup>34</sup>P. Kahl, S. Wall, C. Witt, C. Schneider, D. Bayer, A. Fischer, P. Melchior, M. Horn-von Hoegen, M. Aeschlimann, and F. J. Meyer zu Heringdorf, Plasmonics 9, 1401–1407 (2014).
- <sup>35</sup>J. Seo, H.-H. Nahm, H.-S. Park, S. Yun, J. H. Lee, Y.-J. Kim, Y.-H. Kim, and C.-H. Yang, Phys. Rev. B **108**, 014103 (2023).
- <sup>36</sup>G. F. Nataf and M. Guennou, J. Phys.: Condens. Matter 32, 183001 (2020).
- <sup>37</sup>I. Gaponenko, S. Cherifi-Hertel, U. Acevedo-Salas, N. Bassiri-Gharb, and P. Paruch, Sci. Rep. 12, 165 (2022).
- <sup>38</sup>M. Delor, H. L. Weaver, Q. Yu, and N. S. Ginsberg, Nat. Mater. **19**, 56 (2020).
- <sup>39</sup> Z. Guo, Y. Wan, M. Yang, J. Snaider, K. Zhu, and L. Huang, Science 356, 59 (2017).
- <sup>40</sup> M. Dąbrowski, Y. Dai, and H. Petek, Chem. Rev. **120**, 6247 (2020).
- <sup>41</sup>T. J. Davis, D. Janoschka, P. Dreher, B. Frank, F.-J. Meyer Zu Heringdorf, and H. Giessen, Science 368, eaba6415 (2020).
- <sup>42</sup>R. Tromp, J. Hannon, A. Ellis, W. Wan, A. Berghaus, and O. Schaff, Ultramicroscopy **110**, 852 (2010).
- <sup>43</sup>J. L. Spellberg, L. Kodaimati, P. P. Joshi, N. Mirzajani, L. Liang, and S. B. King, Sci. Adv. 10, eado2136 (2024).
- <sup>44</sup>J. Miyawaki, S. Yamamoto, Y. Hirata, M. Horio, Y. Harada, and I. Matsuda, AAPPS Bull. 31, 25 (2021).
- <sup>45</sup>G. C. Schatz and M. A. Ratner, *Quantum Mechanics in Chemistry*, 1st ed. (Dover Publications, New York, 2002).

- <sup>46</sup>A. Szabo and N. S. Ostlund, *Modern Quantum Chemistry: Introduction to Advanced Electronic Structure Theory* (Dover Publications, New York, 1996).
- <sup>47</sup> K. Sato and T. Ishibashi, Front. Phys. 10, 946515 (2022).
- <sup>48</sup>D. C. Harris and M. D. Bertolucci, *Symmetry and Spectroscopy: An Introduction to Vibrational and Electronic Spectroscopy* (Dover Publications, Inc., 1989).
- <sup>49</sup>P. Li and I. Appelbaum, Phys. Rev. B **90**, 115439 (2014).
- <sup>50</sup> X. Ling, S. Huang, E. H. Hasdeo, L. Liang, W. M. Parkin, Y. Tatsumi, A. R. T. Nugraha, A. A. Puretzky, P. M. Das, B. G. Sumpter, D. B. Geohegan, J. Kong, R. Saito, M. Drndic, V. Meunier, and M. S. Dresselhaus, Nano Lett. 16, 2260 (2016).
- <sup>51</sup> P. M. Beaujuge and J. M. J. Fréchet, J. Am. Chem. Soc. 133, 20009 (2011).
- <sup>52</sup>Z. Guo, D. Lee, R. D. Schaller, X. Zuo, B. Lee, T. Luo, H. Gao, and L. Huang, J. Am. Chem. Soc. **136**, 10024 (2014).
- <sup>53</sup> P. P. Joshi, R. Li, J. L. Spellberg, L. Liang, and S. B. King, Nano Lett. **22**, 3180 (2022).
- <sup>54</sup>F. Niefind, A. Neff, S. C. B. Mannsfeld, A. Kahnt, and B. Abel, Phys. Chem. Chem. Phys. 21, 21464 (2019).
- <sup>55</sup>F. Niefind, S. Karande, F. Frost, B. Abel, and A. Kahnt, Nanoscale Adv. 1, 3883 (2019).
- <sup>56</sup>F. Crameri, Scientific colour maps, 2023.
- <sup>57</sup>F. Crameri, G. E. Shephard, and P. J. Heron, Nat. Commun. **11**, 5444 (2020).
- <sup>58</sup>S. Polisetty, J. Zhou, J. Karthik, A. R. Damodaran, D. Chen, A. Scholl, L. W. Martin, and M. Holcomb, J. Phys.: Condens. Matter 24, 245902 (2012).
- <sup>59</sup>S. Biswas, J. Wong, S. Pokawanvit, W.-C. D. Yang, H. Zhang, H. Akbari, K. Watanabe, T. Taniguchi, A. V. Davydov, F. H. da Jornada, and H. A. Atwater, ACS Nano 17, 23692 (2023).
- <sup>60</sup> X. Xu, Q. Song, H. Wang, P. Li, K. Zhang, Y. Wang, K. Yuan, Z. Yang, Y. Ye, and L. Dai, ACS Appl. Mater. Interfaces 9, 12601 (2017).
- <sup>61</sup>S. Puebla, R. D'Agosta, G. Sanchez-Santolino, R. Frisenda, C. Munuera, and A. Castellanos-Gomez, npj 2D Mater. Appl. 5, 37 (2021).
- 62 C. Dias and D. Das-Gupta, J. Appl. Phys. 74, 6317 (1993).
- <sup>63</sup> R. K. Vasudevan, N. Balke, P. Maksymovych, S. Jesse, and S. V. Kalinin, Appl. Phys. Rev. 4, 021302 (2017).
- <sup>64</sup> K. Chang, F. Küster, B. J. Miller, J.-R. Ji, J.-L. Zhang, P. Sessi, S. Barraza-Lopez, and S. S. Parkin, Nano Lett. **20**, 6590 (2020).
- <sup>65</sup>Z. Chen, W. Fu, L. Wang, W. Yu, H. Li, C. K. Y. Tan, I. Abdelwahab, Y. Shao, C. Su, M. Sun, B. Huang, and K. P. Loh, Adv. Sci. 8, 2100713 (2021).
- <sup>66</sup>J. Gonnissen, D. Batuk, G. F. Nataf, L. Jones, A. M. Abakumov, S. Van Aert, D. Schryvers, and E. K. Salje, Adv. Funct. Mater. 26, 7599 (2016).
- <sup>67</sup>H. Schmid, Ferroelectric Ceramics: Tutorial Reviews, Theory, Processing, and Applications (Springer, 1993), pp. 107–126.
- <sup>68</sup> N. Barrett, J. E. Rault, J. L. Wang, C. Mathieu, A. Locatelli, T. O. Mentes, M. A. Niño, S. Fusil, M. Bibes, A. Barthélémy, D. Sando, W. Ren, S. Prosandeev, L. Bellaiche, B. Vilquin, A. Petraru, I. P. Krug, and C. M. Schneider, J. Appl. Phys. 113, 187217 (2013).
- <sup>69</sup> A. Sander, M. Christl, C.-T. Chiang, M. Alexe, and W. Widdra, J. Appl. Phys. 118, 224102 (2015).
- <sup>70</sup> M. B. Holcomb, L. W. Martin, A. Scholl, Q. He, P. Yu, C.-H. Yang, S. Y. Yang, P.-A. Glans, M. Valvidares, M. Huijben, J. B. Kortright, J. Guo, Y.-H. Chu, and R. Ramesh, Phys. Rev. B 81, 134406 (2010).
- <sup>71</sup> T. Taniuchi, Y. Motoyui, K. Morozumi, T. C. Rödel, F. Fortuna, A. F. Santander-Syro, and S. Shin, Nat. Commun. 7, 11781 (2016).
- <sup>72</sup> M. Kronseder, J. Minár, J. Braun, S. Günther, G. Woltersdorf, H. Ebert, and C. H. Back, Phys. Rev. B 83, 132404 (2011).
- <sup>73</sup>E. Elahi, G. Dastgeer, G. Nazir, S. Nisar, M. Bashir, H. Akhter Qureshi, D.-k. Kim, J. Aziz, M. Aslam, K. Hussain, M. A. Assiri, and M. Imran, Comput. Mater. Sci. 213, 111670 (2022).
- <sup>74</sup> A. V. Papavasileiou, M. Menelaou, K. J. Sarkar, Z. Sofer, L. Polavarapu, and S. Mourdikoudis, Adv. Funct. Mater. 34, 2309046 (2024).
- <sup>75</sup>Q. H. Wang, A. Bedoya-Pinto, M. Blei, A. H. Dismukes, A. Hamo, S. Jenkins, M. Koperski, Y. Liu, Q.-C. Sun, E. J. Telford, H. H. Kim, M. Augustin, U. Vool, J.-X. Yin, L. H. Li, A. Falin, C. R. Dean, F. Casanova, R. F. L. Evans, M. Chshiev, A. Mishchenko, C. Petrovic, R. He, L. Zhao, A. W. Tsen, B. D. Gerardot, M. Brotons-Gisbert, Z. Guguchia, X. Roy, S. Tongay, Z. Wang, M. Z. Hasan, J. Wrachtrup, A. Yacoby, A. Fert, S. Parkin, K. S. Novoselov, P. Dai, L. Balicas, and E. J. G. Santos, ACS Nano 16, 6960 (2022).

- <sup>76</sup> E. Bauer, R. Belkhou, S. Cherifi, A. Locatelli, A. Pavlovska, and N. Rougemaille, J. Vac. Sci. Technol. B 25, 1470 (2007).
- <sup>77</sup> H. Ebert, Rep. Prog. Phys. **59**, 1665 (1996).
- <sup>78</sup>C. Zhou, J. Xu, T. Wu, and Y. Wu, APL Mater. 11, 080902 (2023).
- <sup>79</sup>T. Nakagawa and T. Yokoyama, J. Electron Spectrosc. Relat. Phenom. 185, 356 (2012).
- <sup>80</sup> K. Hild, G. Schönhense, H. J. Elmers, T. Nakagawa, T. Yokoyama, K. Tarafder, and P. M. Oppeneer, Phys. Rev. B 82, 195430 (2010).
- <sup>81</sup> G. K. L. Marx, H. J. Elmers, and G. Schönhense, Phys. Rev. Lett. **84**, 5888 (2000).
- 82 W. Kuch and C. M. Schneider, Rep. Prog. Phys. 64, 147 (2001).
- <sup>83</sup> J. Henk, T. Scheunemann, S. V. Halilov, and R. Feder, J. Phys.: Condens. Matter 8, 47 (1996).
- <sup>84</sup>T. Jauk, H. Hampel, J. Walowski, K. Komatsu, J. Kredl, E. I. Harris-Lee, J. K. Dewhurst, M. Münzenberg, S. Shallcross, S. Sharma, and M. Schultze, arXiv.2405.12690 (2024).
- <sup>85</sup>J. Chen, T. Eul, L. Lyu, Y. Li, X. Hu, X. Ning, S. Wang, M. Aeschlimann, and Q. Gong, Opto-Electron. Sci. 1, 210011 (2022).
- <sup>86</sup> R. Fujita, P. Bassirian, Z. Li, Y. Guo, M. A. Mawass, F. Kronast, G. Van Der Laan, and T. Hesjedal, ACS Nano 16, 10545 (2022).
- <sup>87</sup> H. Zhang, R. Chen, K. Zhai, X. Chen, L. Caretta, X. Huang, R. V. Chopdekar, J. Cao, J. Sun, J. Yao, R. Birgeneau, and R. Ramesh, Phys. Rev. B 102, 064417 (2020).

- <sup>88</sup> W. Ge, R. Beanland, M. Alexe, Q. Ramasse, and A. M. Sanchez, Microstructures 3, 2023026 (2023).
- <sup>89</sup> K. M. Boergens, G. Wildenberg, R. Li, L. Lambert, A. Moradi, G. Stam, R. Tromp, S. J. v. d. Molen, S. B. King, and N. Kasthuri, bioRxiv:09.05.556423 (2023).
- <sup>90</sup> R. Li, G. Wildenberg, K. Boergens, Y. Yang, K. Weber, J. Rieber, A. Arcidiacono, R. Klie, N. Kasthuri, and S. B. King, ChemBioChem 2024, e202400311.
- <sup>91</sup> D. M. Evans, V. Garcia, D. Meier, and M. Bibes, Phys. Sci. Rev. 5, 20190067 (2020).
- <sup>92</sup>M. Fiebig, T. Lottermoser, D. Meier, and M. Trassin, Nat. Rev. Mater. 1, 16046 (2016).
- <sup>93</sup> H. Wang, Y. Wen, H. Zeng, Z. Xiong, Y. Tu, H. Zhu, R. Cheng, L. Yin, J. Jiang, B. Zhai, C. Liu, C. Shan, and J. He, "2D ferroic materials for nonvolatile memory applications," Adv. Mater. (published online 2023).
- 94B. Watts, T. Schuettfort, and C. R. McNeill, Adv. Funct. Mater. 21, 1122 (2011).
- 95 L. Li, L. Xie, and X. Pan, Rep. Prog. Phys. 82, 126502 (2019).
- <sup>96</sup>D. Kumar, T. Jin, R. Sbiaa, M. Kläui, S. Bedanta, S. Fukami, D. Ravelosona, S.-H. Yang, X. Liu, and S. Piramanayagam, Phys. Rep. 958, 1 (2022).
- <sup>97</sup>J. Rieger, A. Ghosh, J. L. Spellberg, C. Raab, A. Mohan, P. P. Joshi, and S. B. King, chemRxiv:2024-sl7t4 (2024).